Applied Surface Science 508 (2020) 145129

Contents lists available at ScienceDirect

Applied Surface Science

journal homepage: www.elsevier.com/locate/apsusc

Full Length Article

Packing density, homogeneity, and regularity: Quantitative correlations between topology and thermoresponsive morphology of PNIPAM-co-PAA microgel coatings

Camden Cutright[a,1], Zach Brotherton[a,1], Landon Alexander[a], Jacob Harris[a], Kaihang Shi[a], Saad Khan[a], Jan Genzer[a], Stefano Menegatti[a,b,*]

[a] Department of Chemical and Biomolecular Engineering, North Carolina State University, Raleigh, NC 27695-7905, United States
[b] Biomanufacturing Training and Education Center (BTEC), North Carolina State University, Raleigh, NC 27695-7928, United States

ARTICLE INFO

Keywords:
Stimuli-responsive microgels
Self-assembled monolayers
Spin coating
Particle interactions
Particle packing

ABSTRACT

This study investigates the formation of monolayers of microgel particles comprising poly[(N-isopropylacrylamide)-co-(acrylic acid)] on solid substrates, their surface morphology, and stimuli-responsiveness. Crosslinked microgels with different chemical composition were produced to show a broad range of responses in hydrodynamic radius and degree of self-assembly with temperature and pH. Microgels were deposited on silicon wafers primed with a bilayer of poly(octadecene-alt-maleic anhydride) and polyethyleneimine by either incubation or spin coating of aqueous suspension of microgels at different temperature and pH. The characterization of the microgel-coated wafers led to the identification of three metrics describing microgel arrangement: density (ρ); heterogeneity (H), which correlates strongly with ρ and depends on deposition temperature and pH with statistical significance, but not on microgel composition; and packing efficiency (PE), which portrays the regularity of microgel arrangement and exhibits no correlation with ρ nor H. The values of ρ, H, and PE calculated for *in silico* models of microgel coatings confirmed that these three metrics portray distinct characteristics of surface topology. Finally, profilometry analysis showed that microgel coatings respond to thermal stimuli with sensible variations in surface roughness; notably, the thermal variation of roughness correlates strongly with ρ and H, and to a lesser extent with PE.

1. Introduction

Stimuli-responsive surface coatings are utilized in numerous applications, ranging from water repellency [1,2] to biorecognition and biosensing [3,4], and development of substrates for cell culture or tissue scaffolds for regenerative medicine [5–7]. Central to these technologies is the use of hydrophilic and biocompatible polymers that are amenable to either physical or chemical conjugation methods, and, most importantly, respond to external stimuli with reversible changes in their physicochemical properties (*e.g.*, morphology, wettability and phase behavior, as well as optical and mechanical properties) [8–17].

Among the polymers of technical relevance (*i.e.*, abundant availability and low cost), poly(N-isopropylacrylamide) (pNIPAm) [18–20] poly(acrylic acid) (pAA), and their copolymers represent the most prominent examples. pNIPAm is a water-soluble polymer that undergoes a reversible lower critical solution temperature (LCST) phase transition in water at ~32 °C [21] While at temperatures below LCST free pNIPAm chains are fully hydrated in solution, they collapse at temperatures above LCST and phase separate into polymer-rich aggregates [22]. Copolymers of NIPAm and AA demonstrate a hybrid behavior, where the LCST increases with increasing AA/NIPAm monomer ratio and with decreasing the pH of the aqueous solution. This is because interactions with surrounding water molecules are increased with the introduction of negatively charged AA monomers, requiring higher temperatures to disrupt the network of hydrogen bonds needed to induce phase transition [23]. These properties have been utilized to construct hydrogel microparticles (microgels) by covalent crosslinking of NIPAm and AA with Bisacrylamide [24,25]. These microgels have been integrated in engineered systems for the removal of toxic metal ions from wastewaters [26], catalysis [27], drug release [28], development of cell mimetics [29], biosensors [30], wound healing and coating of prosthetics [31,32]. Such applications

* Corresponding author at: Engineering Building 1 (EBI), 911 Partners Way, Raleigh, NC 27695, United States.
E-mail address: smenega@ncsu.edu (S. Menegatti).
[1] Indicates equal contribution.

https://doi.org/10.1016/j.apsusc.2019.145129
Received 3 October 2019; Received in revised form 26 November 2019; Accepted 18 December 2019
Available online 21 December 2019
0169-4332/

require accurate control of the physicochemical behavior of the microgels in response to environmental stimuli (*i.e.*, temperature and pH) and, most importantly, of the density and packing homogeneity of the microgel particle assemblies on the substrate surface.

Numerous studies have investigated how the chemical composition of microgels (*i.e.*, NIPAm/AA ratio and concentration of the cross-linkers) and their method of deposition on solid surfaces determine the stimuli-responsive behavior of the resulting microgel layer in terms of thickness, morphology, elasticity, and wettability [33–35]. Most publications related to this topic have relied on using silicon wafers coated with cationic polymers as a primer, coating the microgels onto the substrate, and varying the temperature and pH of the aqueous environment. Analytical methods involved water contact angle measurements to probe wettability, atomic-force microscopy (AFM) and scanning-force microscopy (SFM) to probe surface morphology and elasticity (Young's modulus) of the microgel layer [36].

These groundbreaking studies, however, have not described the morphology of microgel coatings beyond areal density and thickness and have not linked quantitatively the observed macroscopic properties to the microgel characteristics (*i.e.*, chemical composition) or the deposition method (*i.e.*, spin-coating or adsorption from solution), and deposition conditions (*i.e.*, pH and temperature of the aqueous microgel suspension). Review of the literature data, however, suggests that homogeneity and geometrical regularity – together with density – are key parameters to describe the 2D arrangement of the hydrogels, and depend significantly upon chemical composition as well as deposition method and environment. To fill this lacune, this study presents a toolbox to derive quantitative correlations connecting microgel composition and size, deposition method and environment, and the resulting morphology and stimuli-responsiveness of microgel coatings. To this end, we have developed an algorithm for the acquisition, processing, and analysis of microscopy images of microgel-coated wafers. This algorithm provides three metrics describing the 2D arrangement of microgels, namely *(i)* wafer-average microgel density (ρ); *(ii)* microgel heterogeneity (H), defined as normalized average standard deviation of local microgel density across the wafer substrate; and *(iii)* packing efficiency (PE), derived from the average radial distribution function of microgels on the wafer. The parameter H quantifies the difference in the contribution by the local values of ρ to the wafer-average ρ, thereby providing a measure of heterogeneity of microgel deposition (*i.e.*, higher H represents more heterogeneous microgel deposition). The PE describes the geometrical regularity of microgels surrounding a reference microgel with given ρ and H.

In this study, we constructed an ensemble of 144 specimens by depositing pNIPAm-co-AA microgels of select composition (AA monomer density of either 5%, 10%, or 20%) onto silicon wafers grafted with *n*-octyltrichlorosilane (OTS) and primed with a polymer bilayer of poly(octadecene-alt-maleic anhydride) (POMA) and polyethyleneimine (PEI) (*vide infra*). The deposition was performed by either incubation or spin coating of microgel aqueous suspensions at different temperature (25 °C and 45 °C) and pH (3, 7, and 10) (Fig. 1). We then applied our algorithm to analyze the optical microscopy images of the microgel-coated wafers to calculate the parameters ρ, H, and PE, and evaluated their dependence upon microgel properties and deposition conditions. Our results reveal a strong correlation between H and ρ; in particular, we detect that H decreases exponentially with increasing ρ. The parameters upon which ρ and H depend with statistical significance do not fully overlap; ρ depends strongly upon the combination of deposition method and pH, and the combination of deposition temperature and pH, but not on the microgel chemical composition. H depends upon the deposition temperature and pH, but not on the deposition method. Finally, PE features a strong dependence on the deposition method (incubation or spin coating), which had limited or no bearing on ρ and H; most notably, PE exhibits a weak dependence upon ρ and has no correlation with H. These findings suggest that the proposed metrics ρ, H, and PE portray distinct characteristics of microgel coatings, and ought to be presented together to describe fully their morphology. To corroborate this observation, we calculated the values of ρ, H, and PE for models of microgel coatings generated *in silico* with different ρ (0.612, 0.824, and 1.030 microgels/μm^2) and distribution (random or hexagonal packing). As expected, the values of PE were found to be independent of ρ and H.

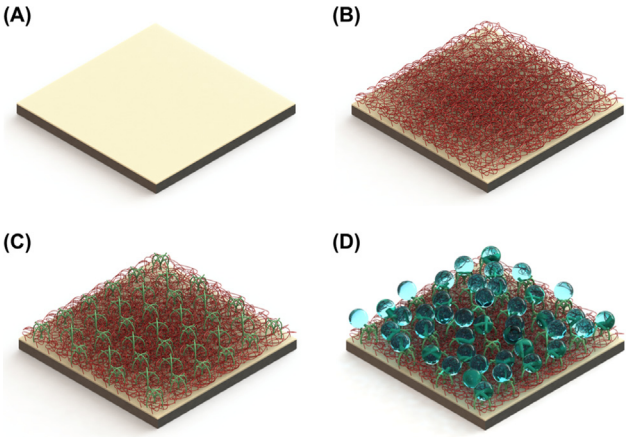

Fig. 1. Construction of microgel-coated wafers. (A) Formation of a monolayer of OTS on a silicon wafer; (B) Deposition of a layer of POMA onto OTS-coated silicon wafer by hydrophobic interaction; (C) Deposition and covalent cross-linking of a layer of PEI onto the underlying POMA layer; (D) Deposition of a monolayer of pNIPAm-co-AA microgels onto the PEI substrate by electrostatic interaction.

We evaluated the thermo-responsive behavior of microgel coatings characterized by different values of ρ, H, and PE by measuring their morphology at different temperatures (25 °C and 45 °C) via non-contact laser profilometry. Our results indicate that microgel coatings respond to thermal stimuli with sensible variations in surface roughness, and, in particular, that the thermal variation of roughness correlates strongly with ρ and H, and to a lesser extent with PE. These results further confirm that ρ, H, and PE portray not only different topological characteristics of microgel coatings, but also their functional morphological properties.

Collectively, these results provide new insight into the mechanisms of self-assembly and stimuli-responsive behavior of microgels on flat solid substrates as it pertains to their chemical composition and deposition conditions (method of deposition, temperature, and pH), and guides the design of surface coatings with desired morphology and behavior.

2. Experimental

2.1. Materials

n-isopropylacrylamide (NIPAm), Acrylic Acid (AA), bis-acrylamide (BIS), ammonium persulfate (APS), *n*-octyltrichlorosilane (OTS), poly (octadecene-alt-maleic anhydride) (POMA), toluene, hexane, tetrachloromethane (CCl_4), sodium carbonate, sodium citrate, phosphate buffer saline (PBS), and poly(ethylene imine) (PEI) were obtained from Sigma Aldrich (St. Louis, MO). Silicon wafers (orientation [100]) were obtained from Silicon Valley Microelectronics (Santa Clara, CA).

2.2. Free radical polymerization (FRP) of microgels

NIPAm was recrystallized from hexanes before use, whereas all other chemicals were used without further purification. The microgels were synthesized via precipitation polymerization in water (100 mL) as described by Brown et al. [36] using varying ratios of NIPAM, AA, and BIS; the total concentration of the monomers was held constant at 100 mM across all reactions. The monomers were initially dissolved in

MilliQ water, and placed in a three-neck flask fitted with a temperature probe, a condenser, and a nitrogen line. After purging with N_2 for one hour at 70 °C, 44 μmol of APS was added to initiate the polymerization. While turbidity was observed within 5 min, the reaction was allowed to continue at 70 °C for 5 h and was then cooled. The resulting solution was filtered through glass wool to remove aggregates and dialyzed against MilliQ water for 72 h to remove unreacted reagents (the dialysis MilliQ water was replaced every 24 h).

2.3. Dynamic light scattering (DLS)

A volume of 10 μL of dialyzed suspension of microgels at 0.3 mg/mL was diluted 100-fold into MilliQ water (resistivity: 18.6 MΩ cm) and placed into disposable 3 mL polypropylene cuvettes. The samples were analyzed by dynamic light scattering (DLS) using a Malvern Nano ZSP instrument. Cumulant analysis of the spectra was performed to determine the z-average size and polydispersity (PDI) of the samples. The data generated were accepted for correlation functions with a plateau above 0.8 and averaged over nine samples to obtain equilibrium size. Microgels in aqueous suspension were characterized over a range of temperatures (21–51 °C) and pH values (2.5–7). For the analysis of pH responsiveness, MilliQ water was replaced with a 10 mM solution of citrate buffer during the dilution process.

2.4. Priming the surface of silicon wafers with an OTS/POMA/PEI substrate layer

Silicon wafers were cut into 1 cm × 1 cm squares, sonicated in toluene, methanol, and acetone, and oxidized in an ultraviolet/ozone (UVO) cleaner (Jelight, Irvine, CA) for 20 min. Afterward, the specimens were washed with MilliQ water and dried to create a Si-OH base layer. The OH-activated wafers were incubated in 10 mL of 1%v/v OTS in 9:1 hexane:CCl_4 overnight to create a self-assembled monolayer (SAM) atop the wafer substrates. All subsequent layers were deposited atop the OTS by spin coating. An ensemble of solutions of POMA in toluene at different concentrations (0.025–10 mg/mL) and PEI in 100 mM carbonate buffer (adjusted to either pH 6, 8, or 10) at different concentrations (0.25–10 mg/mL) were prepared and filtered through a 0.25 μm PTFE filter. The POMA layer was formed by spin coating 100 μL of solution of POMA in toluene (10 mg/mL) at 2000 rpm for 2 min. The second layer was formed by spin coating 100 μL of solution of PEI in 100 mM carbonate buffer at pH 10 (10 mg/mL) at 3000 rpm for 2 min.

2.5. Variable angle spectroscopic ellipsometry (VASE)

The thickness of the OTS, POMA, and PEI layers deposited on the silicon wafers was measured using a VASE ellipsometer (J.A. Woollam, Co., Inc., Lincoln, NE). Prepared samples were visually inspected for opacity, and only the transparent samples were subjected to VASE analysis. A custom fitting model for silane and the Cauchy layer model for POMA and PEI [37] was implemented to analyze the raw data and obtain values of thickness.

2.6. Coating silicon wafers with microgels by incubation

Silicon wafers coated with OTS/POMA/PEI were incubated overnight in a suspension of microgels at 10 mg/mL in different buffered solutions (either 100 mM sodium citrate at pH 3, PBS at pH 7, or 100 mM carbonate buffer at pH 10) at either 25 °C or 45 °C.

2.7. Coating silicon wafers with microgels by spin coating

Silicon wafers coated with OTS/POMA/PEI were initially *vacuum*-sealed on a turntable. A suspension of microgels at 10 mg/mL in different buffered solutions (either 100 mM sodium citrate at pH 3, PBS at pH 7, or 100 mM carbonate buffer at pH 10) was applied atop the wafer surface at a ratio of 200 μL/cm^2 while spinning at 3000 rpm at maintaining the system either 25 °C or 45 °C.

2.8. Water contact angle goniometry

Silicon wafers coated at various stages with OTS, POMA, PEI, and microgels were analyzed using a Ramé-Hart contact angle goniometer equipped with a CCD camera (Model 100-00, Ramé-Hart, Netcong, NJ). Approximately 4–8 μL of distilled water was brought into contact with the wafer, and a camera was used to measure the water contact angle formed by the water bead on the surface of the coated wafer. Eight measurements were taken on each wafer at different locations and averaged.

2.9. Laser scanning microscopy

Microgel-coated wafers were analyzed by non-contact surface profilometry using a laser scanning microscope Keyence VK-X1100 (Osaka, Japan). The microgel coated wafers were initially scored with an surgical scalpel to remove a portion of the coating. The interface of the scored areas was imaged at 150x magnification. Depth scans were performed on dry samples to determine the dry thickness of the polymer layers. Other scored samples were incubated overnight in MilliQ water to swell and placed on a small heating block for thermal regulation. Upon reaching thermal equilibration, depth scans were performed at 150x magnification to determine the thickness and surface profile of the system in the swollen (25 °C) and deswollen (45 °C) state.

3. Results and discussion

3.1. Priming the surface of silicon wafers with a substrate layer of OTS/POMA/PEI

Following published studies [33], we have resolved to prime the surface of silicon wafers with a substrate polymer comprising a tri-layer assemble featuring *n*-octyltrichlorosilane (OTS), poly(octadecene-alt-maleic anhydride) (POMA), and poly(ethylene imine) (PEI). PEI, a cationic polyelectrolyte featuring a combination of primary, secondary, and tertiary amines, has been utilized extensively as a substrate layer to ensure the adhesion of microgel particles. In our system, the condensation of OTS molecules on the silicon wafer results in a self-assembled layer of hydrophobic alkyl (C_8) moieties on which a stable POMA layer can be deposited by hydrophobic adsorption (Fig. 2A). The POMA chains, in turn, present a plenitude of anhydride moieties that enable the conjugation of incoming PEI chains through the formation of stable amide bonds (Fig. 2B). Finally, the secondary and tertiary amines on PEI provide a high density of positive charges that secure stable anchoring of the microgels. Notably, the high density of covalent POMA/PEI crosslinking makes the bilayer resistant to washes with aqueous acid and alkali, and organic solvents.

Silicon wafers were coated with OTS following a method developed in prior work [38], and characterized by ellipsometry and water contact angle (WCA) measurements. Our measurements indicated the formation of a uniform (~1 nm) thick OTS layer atop the silicon wafer through a shift of WCA from 59° (bare silicon oxide) to 105° (OTS-coated wafer), confirming the formation of a hydrophobic surface. Additionally, ellipsometry confirmed a 1 nm thick silane layer atop the silicon wafer.

Following OTS deposition, the subsequent layers of POMA and PEI were formed by spin coating (respectively at 2000 rpm and 3000 rpm for 2 min). A set of samples were prepared by varying the concentration of POMA in toluene between 0.025 and 10 mg/mL, and evaluated by WCA measurements. As anticipated, the coating with POMA at higher concentrations returned surfaces with increasing thickness and hydrophobicity, as indicated by values of WCA dropping from ~103°

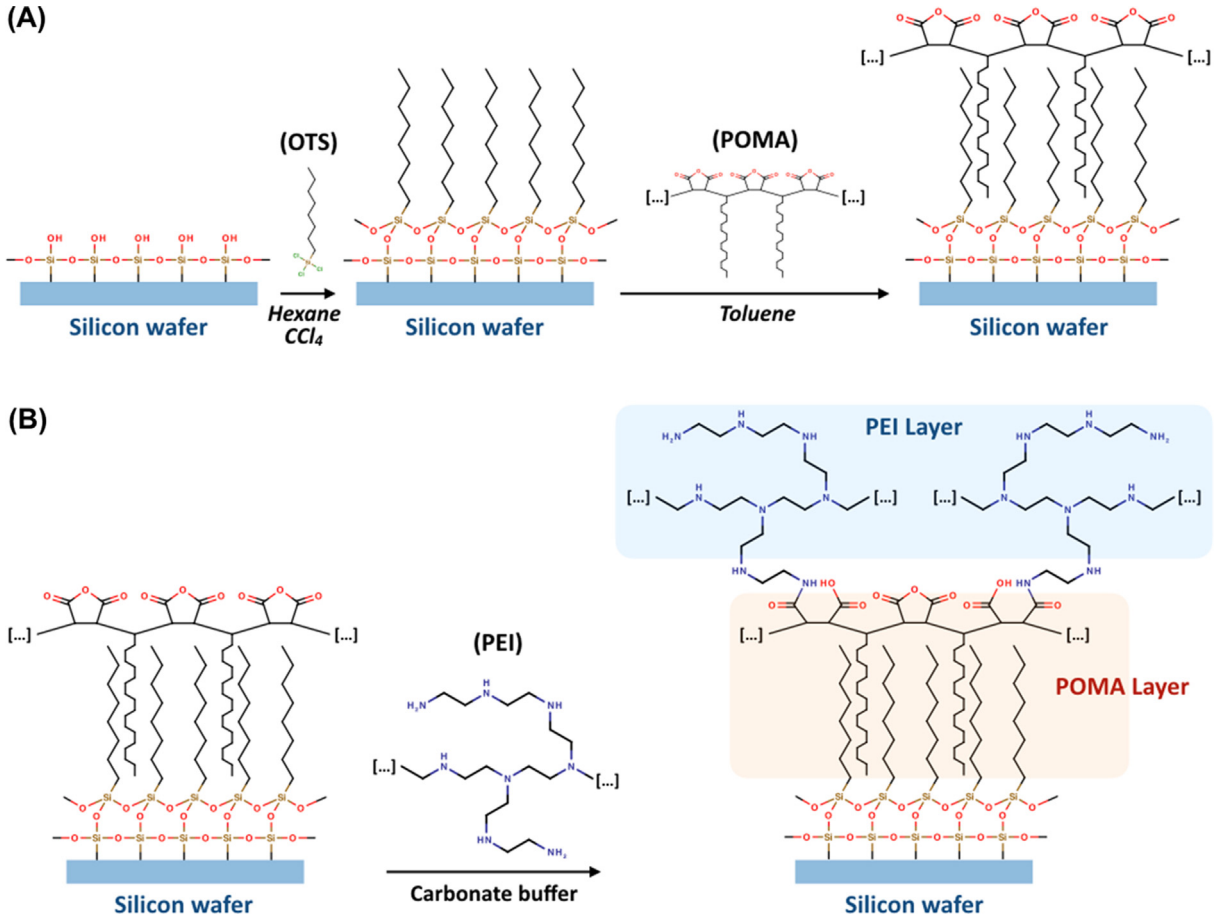

Fig. 2. Construction of OTS/POMA/PEI coatings on top of silicon wafers. (A) A layer of POMA is formed onto OTS-coated silicon wafer via hydrophobic interaction between the octadecyl-(C_{18}) side chain groups of POMA and the octyl-(C_8) chain displayed on the OTS SAM; (B) covalent crosslinking of PEI chains to the underlying POMA layer by formation of amide bonds between the primary amines of PEI and the maleic anhydride moieties of POMA.

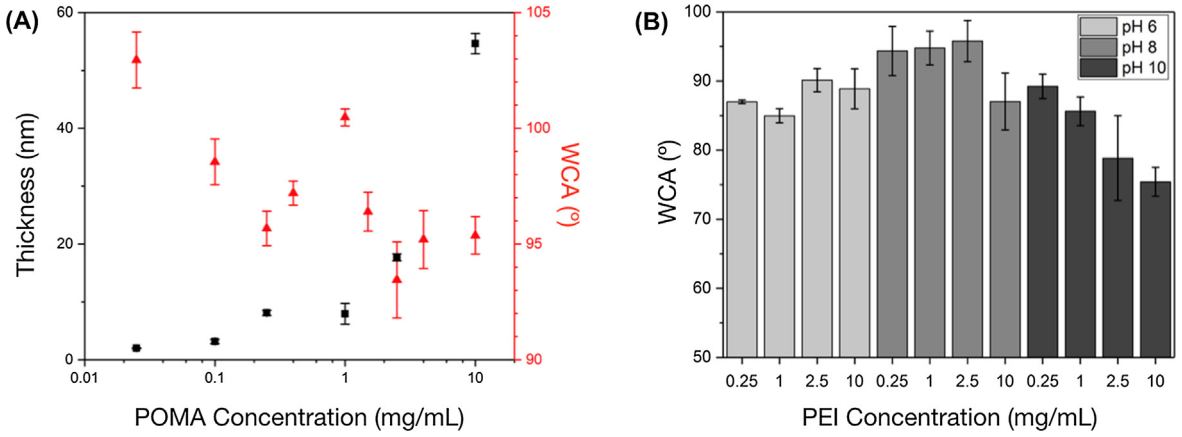

Fig. 3. Characterization of OTS/POMA and OTS/POMA/PEI coatings on silicon wafers. (A) Thickness (left ordinate) and water contact angle (WCA, right ordinate) of the POMA layer obtained on OTS-silicon wafer obtained by spin coating POMA solutions in toluene at concentrations varying in the range 0.25–10 mg/mL, as obtained from ellipsometry measurements. (B) Values of WCA measured on OTS/POMA/PEI-coated wafers obtained via spin coating of PEI solutions at different concentrations (0.025–10 mg/mL) and pH (100 mM carbonate buffer at pH 6, pH 8, and pH 10) onto POMA/OTS-silicon wafers constructed by spin coating 10 mg/mL solution of POMA in toluene onto OTS-coated silicon wafers.

(0.025 mg/mL) to ~95° (10 mg/mL) (Fig. 3A). We also observed that, while relying on non-covalent hydrophobic binding only, the adhesion of the POMA layer on the OTS-silicon wafer resists to washing with water, aqueous acids and alkali, and organic solvents. Ellipsometry and WCA measurements showed no variations of surface properties upon treatment across the entire set of POMA-coated wafers. The WCA values suggest that the POMA-coated wafers constructed with diluted POMA solutions (< 1 mg/mL) feature heterogeneous coating, with gaps of uncoated OTS as shown in Fig. 1S-A – 1S-C, which are unsuitable for the subsequent PEI and microgel depositions. We therefore resolved to utilize concentrated POMA solutions (10 mg/mL, Fig. 1S-D) to obtain a uniform coating on the OTS-silicon wafers.

As for POMA, the deposition of PEI by spin coating was also attempted at different conditions, specifically PEI concentration

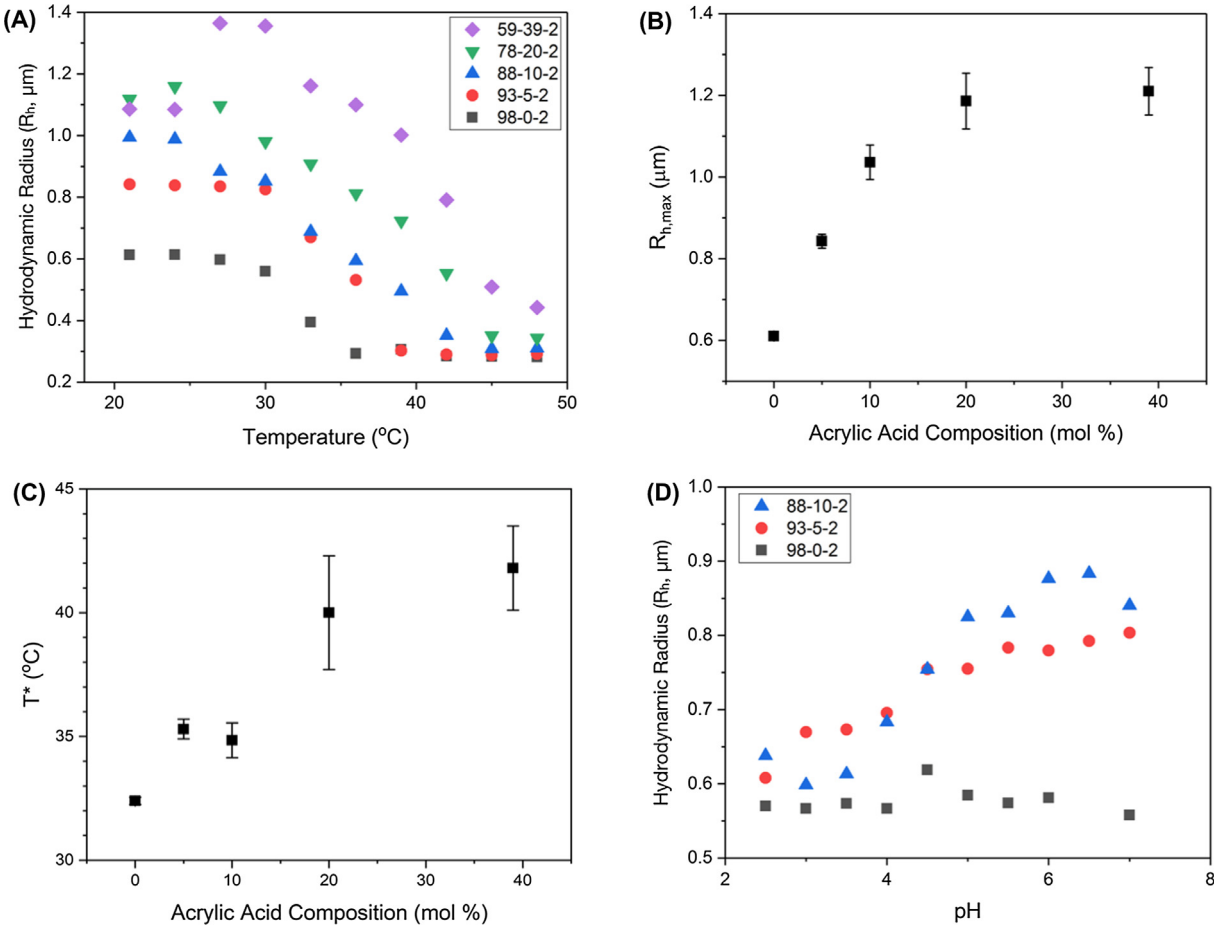

Fig. 4. Characterization of microgels in aqueous suspensions at different temperatures and pH. (A) Values of hydrodynamic radius (R_h) *vs.* temperature for microgels constructed with different NIPAm/AA monomer ratios; the R_h was obtained by DLS analysis of the microgels in aqueous suspension while increasing the temperature from 21 °C to 51 °C. The data of R_h *vs.* temperature were fitted using a hyperbolic tangent equation (Table 1S) to derive the values of (B) maximum hydrodynamic radius ($R_{h,max}$) and (C) T* for the ensemble of microgels constructed using different NIPAm/AA monomer ratios. (D) Values of hydrodynamic radius (R_h) *vs.* pH for microgels constructed with different NIPAm/AA monomer ratios; the R_h was obtained by DLS analysis of the microgels in aqueous suspension while decreasing the pH from 7 to 2.5. The numbers in the legend in (A) indicate the NIPAm-AA-BIS monomer ratios.

(0.025–10 mg/mL) and pH of the buffered aqueous solution (100 mM carbonate buffer at pH 6, 8, and 10). The characterization of the final PEI-POMA-OTS-silicon wafers by WCA measurements indicates that both the concentration and the pH of the solution impact significantly the degree and uniformity of surface coverage (Fig. 3B). In particular, the PEI solution at 10 mg/mL and pH 10 returned the most uniform hydrophilic surface, and was therefore adopted for constructing all the OTS/POMA/PEI primers on silicon wafers utilized in this work.

3.2. Characterization of the microgel in aqueous suspension at different temperatures and pH

Microgels with different ratios of N-isopropylacrylamide (NIPAm) and Acrylic Acid (AA) monomers were synthesized by free radical polymerization [39]. The combination of NIPAm and AA endows the microgels with responsiveness to both thermal and pH stimuli, as shown in prior work [34]. We employed dynamic light scattering (DLS) to measure the diameter variation of the microgels over a range of temperatures and pH values of the aqueous suspension. As anticipated, the data show a downward trend in the hydrodynamic radius (R_h) with increasing temperature (Fig. 4A). This collapse in R_h is caused by the LCST-type transition triggered by the shrinkage of the NIPAm segments, which induces hydrophobic aggregation of the chains at elevated temperatures and, consequently, shrinkage of the particles. The values of R_h of the microgels *vs.* temperature of the aqueous suspension were fitted using a hyperbolic tangent function (Fig. 2S), from which the values of maximum hydrodynamic radius ($R_{h,max}$) and the gel LCST were obtained for the microgels of different monomer compositions (Table S1). $R_{h,max}$ corresponds to the asymptotic value of R_h ($T \rightarrow \infty$), while the gel T* is the value of temperature corresponding to the inflection point in the R_h curve. Both $R_{h,max}$ and the gel T* increase with increasing the AA/NIPAm monomer ratio (Fig. 4B and C). The negatively charged carboxyl groups displayed by the AA monomers caused an increase in the inherent hydrophilicity of the polymer chains as well as their relative distance by electrostatic repulsion resulted in larger particles. Higher temperatures were thus required to attain the hydrophobically-driven collapse of the chains. These results collectively indicate that the size and thermal responsiveness of the particles can be tailored as desired by adjusting the monomer ratio. Similar behavior was observed in response to pH values, although the data trend was not as well defined as in the thermal treatment. As the pH of the aqueous suspensions decreases, the negative charge on the AA monomers progressively decreases, resulting in lower electrostatic repulsion among polymers and lower inherent hydrophilicity of the chains. Accordingly, the $R_{h,max}$ of the microgels and the width of the pH window across which the size transition occurs are magnified at higher values of the AA/NIPAm monomer ratio (Fig. 4D). Based on these results, we resolved to utilize the microgels constructed with NIPAm-AA-BIS molar monomer ratios of 93-5-2, 88-10-2, and 78-20-2.

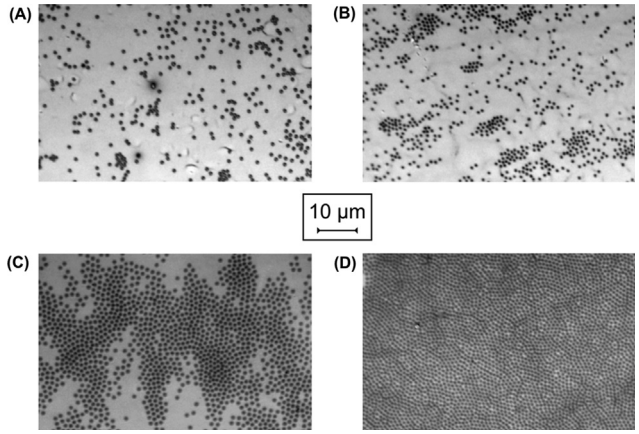

Fig. 5. Example images of microgel-coated wafers. (A) 88-10-2 microgels spin-coated at pH 10 and 45 °C; (B) 88-10-2 microgels spin-coated at pH 10 and 25 °C; (C) 93-5-2 microgels spin-coated at pH 3 and 45 °C; and (D) 78-20-2 microgels spin-coated at pH 3 and 45 °C. The numbers indicate the NIPAm-AA-BIS monomer ratios.

3.3. Formation and characterization of microgel monolayers on OTS/POMA/PEI coatings on silicon wafers

Microgels with three selected monomer composition (93-5-2, 88-10-2, and 78-20-2) were deposited on the OTS/POMA/PEI-coated wafers using different methods and conditions. Specifically, we compared *(i)* incubation *vs.* spin coating, *(ii)* deposition at 25 °C *vs.* 45 °C, *(iii)* deposition at pH 3 *vs.* 7 *vs.* 10. Every combination was conducted in 4 technical replicates, resulting in an ensemble of 144 samples (*i.e.*, 3 monomer ratios × 2 deposition methods × 2 temperature values × 3 pH values × 4 replicates) that were individually imaged by optical microscopy in the reflection mode. All microscopy images were taken in grayscale in increase contrast. Four representative images of microgel-coated wafers are reported in Fig. 5, while the images of all 144 wafers are found in Fig. 3S.1 − 3S.36.

The images were processed using our algorithm "ImProVisED" (Image Processing, Visualization, and Evaluation of Density; a detailed description of the algorithm is provided in SI 1) to determine the position of every microgel in a 40 μm × 50 μm reference grid of every wafer image, and calculate three key response parameters for every wafer:

(1) *Wafer-average microgel density* (ρ, microgel/μm^2), calculated as the ratio between the total number of microgels counted within the reference section and the reference area (2000 μm^2).
(2) *Deposition heterogeneity (H)*. The reference section was initially scanned pixel-by-pixel using a sampling window of 2.5 μm × 2.5 μm. As the resolution of the microscope is 10 pixels/μm, we obtained 200,000 scansions per wafer. The values of local ρ in every scanning window were then calculated as the ratio between the number of microgels and the surrounding window (6.25 μm^2). Finally, the nondimensional parameter H was calculated by normalizing the standard deviation of local ρ to the wafer-average ρ.
(3) *Packing efficiency (PE)*. Using our algorithm "CARDFs" (Calculation of Average Radial Distribution Functions; a detailed description of the algorithm is provided in SI 2), the local radial distribution functions (RDFs) were initially calculated from the center of every microgel within the reference section over a circle of 5 μm radius; periodic boundary conditions were applied to account for microgels located on the periphery of the reference section. The average radial distribution function (ARDF) was then evaluated by averaging the local RDFs across the reference section on every wafer and across the 4 technical replicates. The ARDF functions were fit against a dampened sine wave equation, whose fitting parameters were utilized to calculate the values of PE.

The following sections present and discuss separately the dependence of three key response parameters, namely, ρ, H, and PE, upon the deposition parameters, namely, microgel chemical composition, deposition method, temperature, and pH. This analysis sheds light on the mechanisms of microgel interaction and adhesion with the underlying PEI layer and guides to achieve microgel coatings of desired density and packing regularity.

3.4. Evaluation of coating density (ρ)

The values of ρ measured on the wafers prepared at 25 °C and 45 °C are summarized in Fig. 6A and B, respectively. The values calculated by ImProVisED for 132 samples, and the corresponding averages and standard deviations are listed in Table 2S and Table 3S, respectively. Note that image analysis of the 12 microgel-coated wafers prepared by incubation at 45 °C and pH 10 was not possible due to the excessive surface density of the microgels, which was found to be independent of the gel chemical composition (cf. Fig. 3S.24, 3S.30, and 3S.36). These results indicate that the parameter ρ is impacted in different measure by the deposition method and conditions, as it covers a wide range from ~1.7 microgels/μm^2 (93-5-2 microgels deposited by spin coating at 45 °C and pH 10) down to 0.01 microgels/μm^2 (93-5-2 microgels

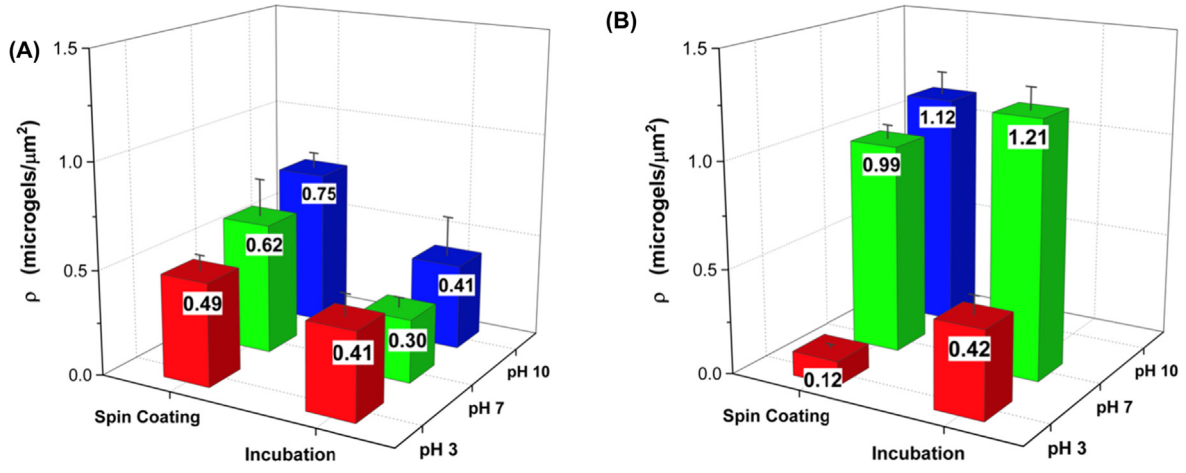

Fig. 6. Wafer-average microgel density ρ calculated on the optical microscopy images on the microgel-coated wafers prepared (A) at 25°C and (B) 45°C using the algorithm ImProVisED.

deposited by incubation at 25 °C and pH 10). Table 4S summarizes the statistical dependence of ρ with the design variables (*i.e.*, microgel composition, and deposition method, temperature, and pH) considered either individually or in combination.

Combination of deposition temperature and pH. Microgel deposition performed above LCST affordshigher density than the deposition below LCST, especially when combined with deposition at pH ≥ 7. Two-dimensional packing of spheres on a flat surface is more efficient, and it approximates the ideal hexagonal packing, as the diameter of the spheres decreases [40]. Accordingly, above their LCST, microgels feature a smaller R_h and are therefore inherently capable of covering the available surface more efficiently, thereby attaining higher values of ρ. Furthermore, when depositing at pH ≥ 7, the electrostatic interaction between the negatively charged microgels and the underlying PEI layer is maximized and secures strong adhesion of the microgels to the underlying substrate. Finally, we note that, while being maintained above LCST during deposition, the temperature of the wafer falls below the LCST before imaging by optical microscopy, thereby allowing the microgels to swell and reach high surface packing density.

Combination of deposition method and environment. Spin coating affords consistently higher density compared to incubation below LCST, whereas above LCST the opposite trend is observed. During spin coating, the microgels are driven downward and outward due to centrifugal forces, thereby mechanically promoting their interaction with the surface compared to the rather passive incubation process. In particular, at T < LCST and low pH, the microgels are soft and can be easily deformed during spin coating and occupy a large area per microgel particle on the wafer and result in lower ρ (Table 3S). Spin coating, characterized by short contact time (< 1 s) of the microgel suspension on the wafer, provides good surface coverage only when sufficient non-covalent interactions are present to promote the microgel/PEI interactions. This is demonstrated by the values of ρ obtained at pH 3, where the gels are electrically neutral. Spin coating at 25 °C, where T < LCST and therefore the isopropylacrylamide and carboxyl groups displayed on the NIPAm and AA monomers, respectively, can form hydrogen bonds, provides good coverage (ρ varies between ~0.6 and 0.8 for 78-20-2 microgels/μm^2 to 0.6–0.9 for 93-5-2 microgels/μm^2). At T > LCST instead, hydrogen bonding weakens, and fewer interactions are left to enable substrate adhesion, resulting in relatively poor coverage (ρ ~ 0.12 microgels/μm^2). Incubation, on the other hand, features a much longer contact time and the resulting values of ρ are strongly affected by the combination of size and charge of the microgels. At T < LCST, where microgels are expanded, ρ decreases with increasing solution pH, and therefore the electrostatic repulsion among the microgels. When incubated at T > LCST, the microgels are smaller ($R_{h,min}$ at 25 °C ~ 0.25–0.5 $R_{h,max}$ at 45 °C) and can, given sufficient time, distribute on the surface in an initial configuration that minimizes electrostatic repulsion. Following incubation, however, the temperature of the wafer falls below the LCST, resulting in an expansion of the microgels and ultimately in a higher effective final density, reaching values of up to 1.2 microgels/μm^2.

Chemical composition of the microgels. Polymer chemical composition and pH also impact density by controlling the charge of the surface charge of the microgels, which determines the strength of microgel adhesion to the PEI layer. When exposed to an acidic environment (pH 3), the microgels carry little-to-no negative charge (the pK_a of the carboxyl group on acrylic acid is ~4.5) and therefore adhere poorly to the strongly positively-charged polycationic underlying PEI substrate. Accordingly, surface coverage at pH 3 is particularly poor when deposition is performed at 45 °C by spin coating (ρ ~ 0.12 microgels/μm^2), where microgels behave as hard hydrophobic spheres and are allowed a very short residence time on the surface during the deposition, compared by incubation, where microgels manage to arrange on the surface and reach a higher packing density (ρ ~ 0.41 microgels/μm^2). When the deposition is carried out at pH 7 or 10, the microgels carry a strong positive charge, and the PEI layer displays a moderate - yet non-negligible - positive charge on the tertiary amine groups (pK_a ~ 10.6), resulting in stronger adhesion and ultimately higher ρ (> 0.9 microgels/μm^2 at 45 °C and > 0.4 microgels/μm^2 at 25 °C). At the same time, it must also be considered that, while moderate negative charge promotes microgel adhesion to the underlying PEI layer, high negative charge prevents it by inter-particle electrostatic repulsion. Accordingly, microgels with monomer composition of 93-5-2 achieve higher ρ (up to 1.683 microgels/μm^2) compared to 88-10-2 and 78-20-2 microgels. Furthermore, 93-5-2 microgels are also smaller than their acrylic acid-rich counterparts, and therefore possess an innate ability to achieve higher packing density when contacted randomly on the wafer surface.

3.5. Evaluation of surface coating heterogeneity (H)

Together with density, the uniformity of microgel deposition on the primed wafers plays a crucial role in the stimuli-responsiveness of the resulting microgel monolayer. The initial survey of the images acquired via optical microscopy analysis of the ensemble of microgel-coated wafers suggested that wafers with lower microgel density feature a rather heterogeneous distribution of the particles compared to wafers with higher microgel density, where the microgel distribution is considerably more regular. To obtain a quantitative assessment of this phenomenon, we developed a parameter of heterogeneity of microgel deposition (H), defined as average standard deviation of local values of ρ across the microgel-coated wafer normalized to the wafer-average ρ. Using ImProVisED, we calculated the parameter H for 132 wafers in the ensemble (the images of the 12 microgel-coated wafers coated by incubation at 45 °C and pH 10 could not be processed) by normalizing the standard deviation of the local values of ρ to the wafer-average ρ (Table 5S). High values of H indicate high heterogeneity of microgel surface coverage, whereas smaller values (H < 0.5) indicate coating homogeneity. The plots of H *vs.* ρ, displayed in Fig. 7A and B for the microgel-coated wafers prepared at 25 °C and 45 °C, show a strong inverse correlation, confirming our initial observation that more densely packed systems are more uniform. Table 6S summarizes the statistical dependence of H with the design variables considered either individually or in combination.

Combination of deposition method and temperature. Both plots in Fig. 7 indicate that spin coating affords a more uniform monolayer of microgels compared to incubation. For example, of the 72 samples deposited at 25 °C, the 36 deposited by spin coating had an average H of 0.65 and 18 of them (50%) had H < 0.5, whereas the 36 deposited by incubation had an average H of 1.45, and 17 of them had H > 1. Further, the 6 least homogeneous samples (H > 2) were all prepared by incubation. Furthermore, statistical analysis across the ensemble of wafers prepared at 25 °C indicated no statistically relevant correlation between H and the monomer composition of the microgels. At 25 °C (T < LCST), the microgels are fully swollen and compressible, and the relative difference in R_h among the microgels of difference composition is limited to 10–15%. The downward force applied by spin coating drives the microgels toward the PEI surface promoting their binding to the underlying PEI layer. Throughout the spin coating process, as microgels adhere to the PEI layer, incoming microgels subsequently fill the uncoated areas, eventually resulting in highly homogeneous coatings. This spontaneous process of coating optimization is more efficient below the corresponding LCST of the different microgel populations and is confirmed by the Keyence analysis of the microgel surface morphology.

Deposition pH. Microgel-coated wafers prepared at 45 °C show a noticeable correlation between H and pH. Of the 60 high temperature samples processed by ImProVisED, those deposited at pH 7 or 10 featured homogenous monolayers (H < 0.5), whereas 8 of the 18 samples deposited at pH 3 showed H > 2. Such dependence of self-assembly on pH is likely a consequence of thermally-induced aggregation of the polymer chains in the microgels. The combination of T > LCST and

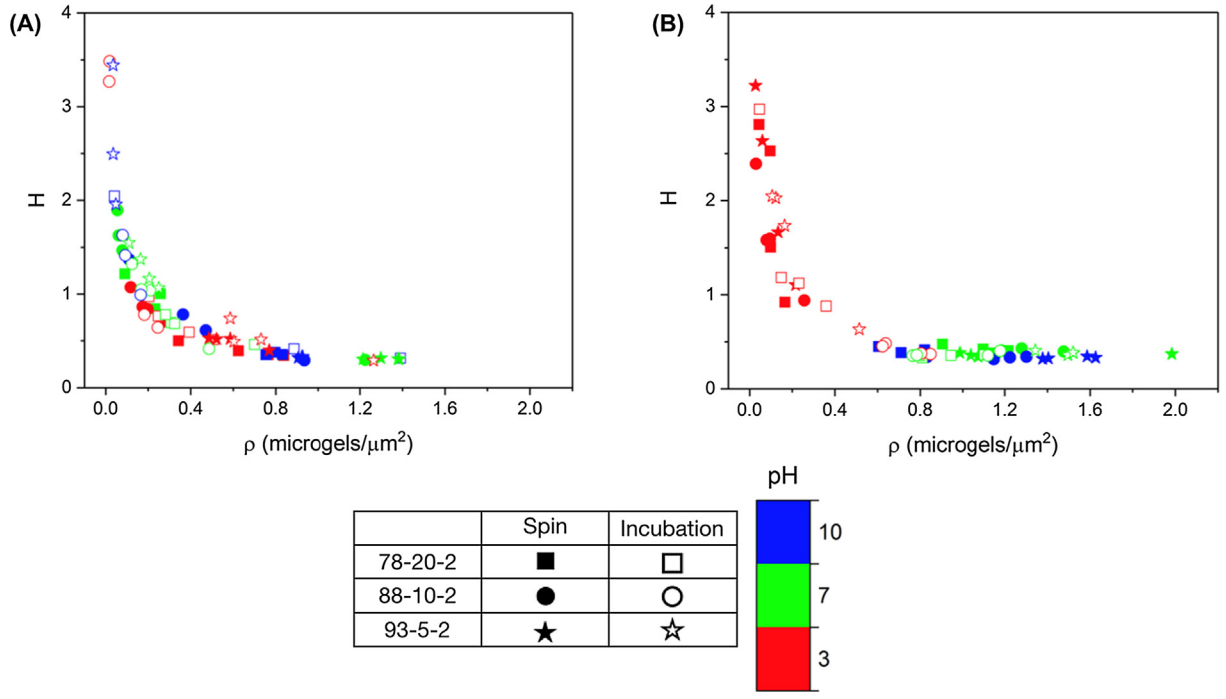

Fig. 7. Correlation of heterogeneity of microgel deposition (H) *vs.* microgel density (ρ) for the microgel-coated wafers prepared (A) at 25°C and (B) 45°C. The numbers in the legend indicate the NIPAm-AA-BIS monomer ratios.

low pH inhibits the ability of the microgel surface to form electrostatic and hydrogen bond interactions with the underlying PEI layer, thereby significantly reducing their ability to form a dense and homogeneous coating. At these conditions, the hydrogels are at their minimum size ($R_h \sim R_{h,min}$) and are more likely to roll on the wafers like hard spheres. This "rolling" mechanism may be more pronounced during spin coating due to centrifugal forces acting on the collapsed uncharged particles. On the contrary, at pH 7 or 10 the hydrogels are highly charged and therefore still capable of binding to the PEI layer. In this scenario, their smaller size promotes efficient packing, resulting in denser and more homogeneous coatings.

3.6. Evaluation of the regularity of microgel surface arrangement (PE)

The parameter H, by portraying the spatial variability of local values of ρ in comparison to the wafer-average ρ, provides a quantitative measure of the homogeneity of microgels distribution. However, it does not inform on the regularity of microgel packing (*i.e.*, long-range order). To gather insight into this aspect, we developed the algorithm CARDFs for calculating the radial distribution function (ARDF) of microgel density averaged among the replicates of microgel-coated wafers (Fig. 3S.1 − 3S.36). The values of ARDFs as a function of radial distance from the reference microgel were interpolated using a dampened sine wave model (Eq. (1)):

$$ARDF = \alpha[e^{-\beta r}sin(\gamma r + \delta) + e^{-\varepsilon r}sin(\zeta r + \eta)] + 1 \quad (1)$$

The parameter α determines the initial amplitude of the function, and describes the probability of having an ordered ring of microgels immediately surrounding a reference microgel; this parameter is therefore only loosely related to the microgel density ρ. The parameters β and ε determine how rapidly the ARDF function decays, and describe the probability that an exterior ring of microgels exists to encircle an interior ring. The parameters γ and ζ determine the frequency of the peaks and describe how closely an exterior ring encircles an interior ring; these parameters measure the density of the regular microgel packing (note that this is not directly related to the wafer-density of the beads but rather to how densely packed the regular arrangements of the microgels are). Finally, the parameters δ and η represent the phase angles at an arbitrary point and determine a shift in the function to provide better fitting of the data; accordingly, these are purely mathematical terms, with no physical meaning. RDF shaped as dampened oscillating functions appear in a variety of fields and applications related to the self-arrangement/assembly/packing of particular materials [41–51]. In this context, the ARDF function can therefore be used to analyze the packing pattern of the microgels. If the microgels are regularly patterned and the microgel patterns are evenly distributed, a perfect damped sinusoidal form of ARDF is achieved around any reference microgel. If the patterns are irregular or unevenly distributed, the form of ARDF reduces to exponential decay. Finally, in those cases where patterning is absent, and microgel packing is random or patchy, the ARDF curve rapidly flattens to unity. Based on these considerations, we define the "packing efficiency" (PE) of a microgel layer on wafers as (Eq. (2)):

$$PE = \alpha\frac{\gamma\cdot\zeta}{\beta\cdot\varepsilon} \quad (2)$$

Higher values of PE indicate densely and regularly packed microgel coatings, whereas lower values of PE are typical of poorly packed coatings.

Using the algorithm CARDFs, we produced 33 ARDFs (Fig. 3S), one for every set of images of microgel-coated wafers, fitted them using Equation (1) to derive the parameters α, β, γ, δ, ε, ζ, and η. ARDF datasets with poor fits were discarded, and the corresponding microgel distributions were considered irregular. For ARDF datasets providing good fits, the PE values varied within a broad range of values, between 0.03 and 38. PE increases with packing regularity, as shown by the 4 example microgel-coated wafers displayed in Fig. 8. At the same time, it should be noted that no explicit correlation between PE and ρ or H was found. Comparing the values of ρ, H, and PE across the 132 measurable samples highlights the differences between the topological properties that these parameters separately describe. Some examples are particularly worthy of mentioning. 78-20-2 microgels deposited at 25 °C by spin coating at pH 3 featured H = 0.4, indicating good homogeneity, but the corresponding ARDF dataset could not be fit, indicating poor

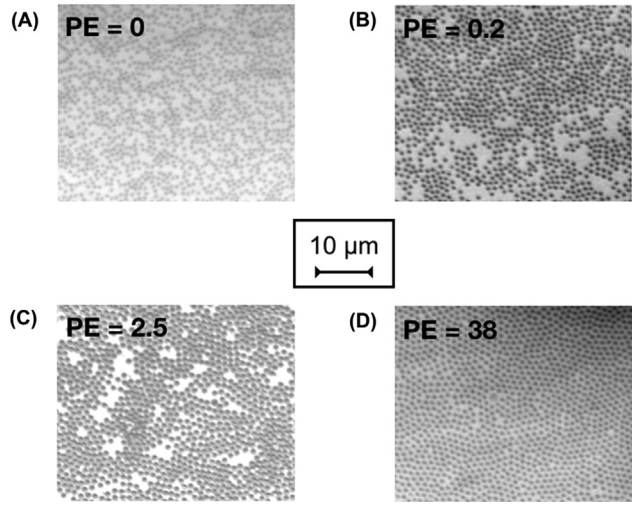

Fig. 8. Examples of microgel-coated wafers with different values of PE, obtained by (A) spin coating of 78-20-2 microgels at pH 3 and 25 °C; (B) spin coating of 93-5-2 microgels at pH 3 and 25 °C; (C) spin coating of 78-20-2 microgels at pH 10 and 45 °C; and (D) spin coating of 93-5-2 microgels at pH 10 and 25 °C. The numbers in the legend indicate the NIPAM-AA-BIS monomer ratios.

packing regularity. Further, 93-5-2 microgels deposited by spin coating at pH 10 achieved high ρ and identical H, but featured much different packing regularity when deposited at 25 °C (PE = 37.968) *vs.* 45 °C (PE = 9.331). Notably, Fig. 4S shows no correlation between H and PE, indicating that homogeneity and regularity of microgel distribution are not correlated.

Reference values of PE were calculated for six model microgel coatings generated *in silico* with different ρ (0.612, 0.824, and 1.030 microgels/μm^2) and distribution (randomly distributed *vs.* hexagonal packing) (Fig. 5S). As expected, the values of PE were found to be very low for randomly distributed microgels (~0.09–0.54) and very high for ordered microgels (~62–121). Notably, PE varied substantially between coatings with identical ρ but different microgel arrangement, while showing almost no variation across the different values of ρ. This corroborates the observation that the geometrical regularity of microgel 2D arrangement portrayed by PE is independent of density and homogeneity of distribution.

Conclusive proof of the distinction between ρ, H, and PE is provided by statistical analysis of the design parameters. Specifically, we performed an ANOVA analysis of the dependence of ρ and H against monomer composition of the microgels, and deposition method and conditions; the resulting effect summary report listing the LogWorth values ($-\log_{10}$(p-value)) of the effects the design variables on ρ and H is reported in Fig. 9. In comparing Tables 4S and 6S, and Fig. 3S, it was first noted that, despite the strong correlation between H and ρ, the parameters upon which ρ and H depend with statistical significance do not fully overlap. First, ρ depends strongly upon the combination of deposition method and pH, as well as deposition temperature and pH, but not on microgel composition (Fig. 9, black bars). H, instead, depends upon deposition temperature and pH, but not on deposition method (Fig. 9, grey bars). Furthermore, PE was found to possess no correlation with either ρ or H (Fig. 4S); PE featured dependence on the deposition method (incubation or spin coating) and microgel composition, which had limited or no bearing on ρ and H. These findings demonstrate that the proposed metrics ρ, H, and PE portray distinct

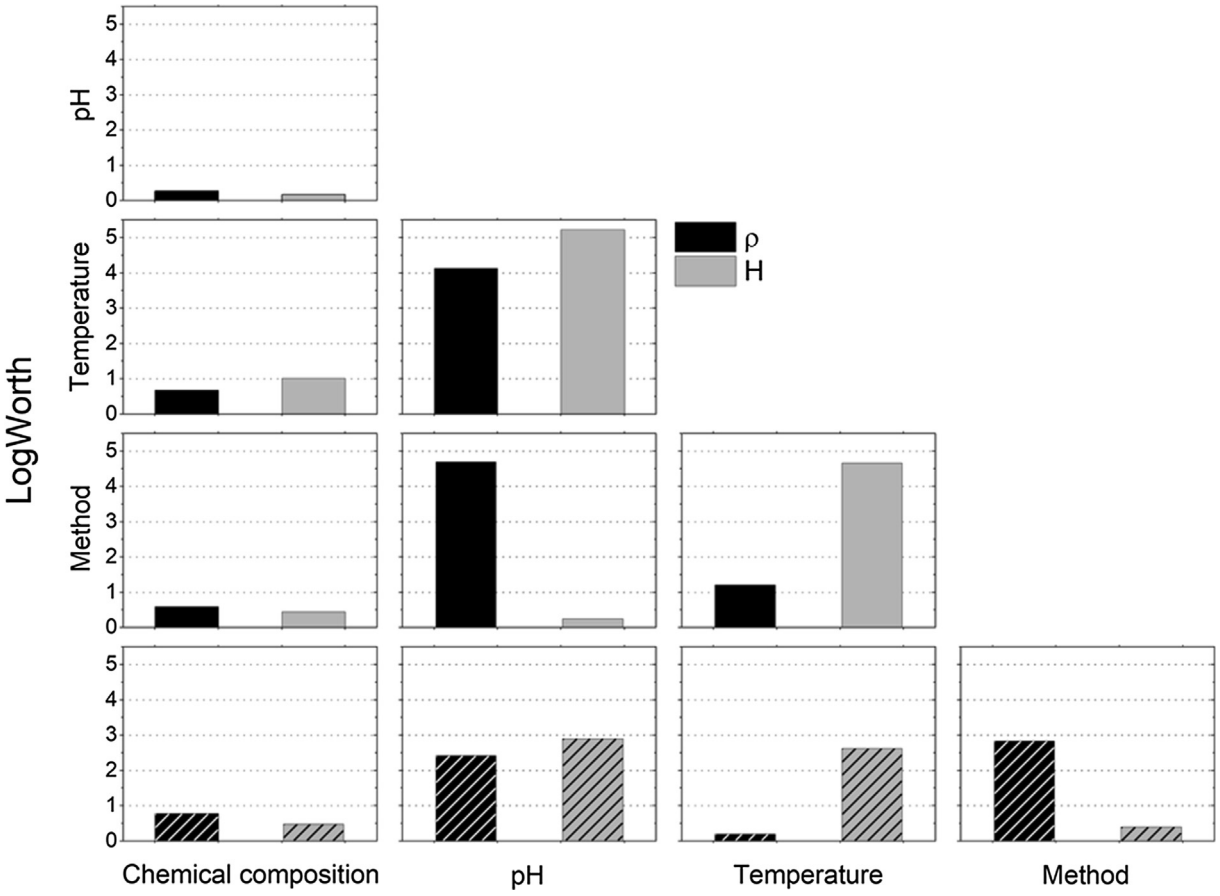

Fig. 9. Statistical correlations of ρ and H upon monomer composition of the microgels, and pH, temperature, and method of deposition (spin coating *vs.* incubation) calculated by ANOVA analysis using JMP®. The resulting logarithmic values of $-\log_{10}$(p-value) are presented in black for ρ and grey for H.

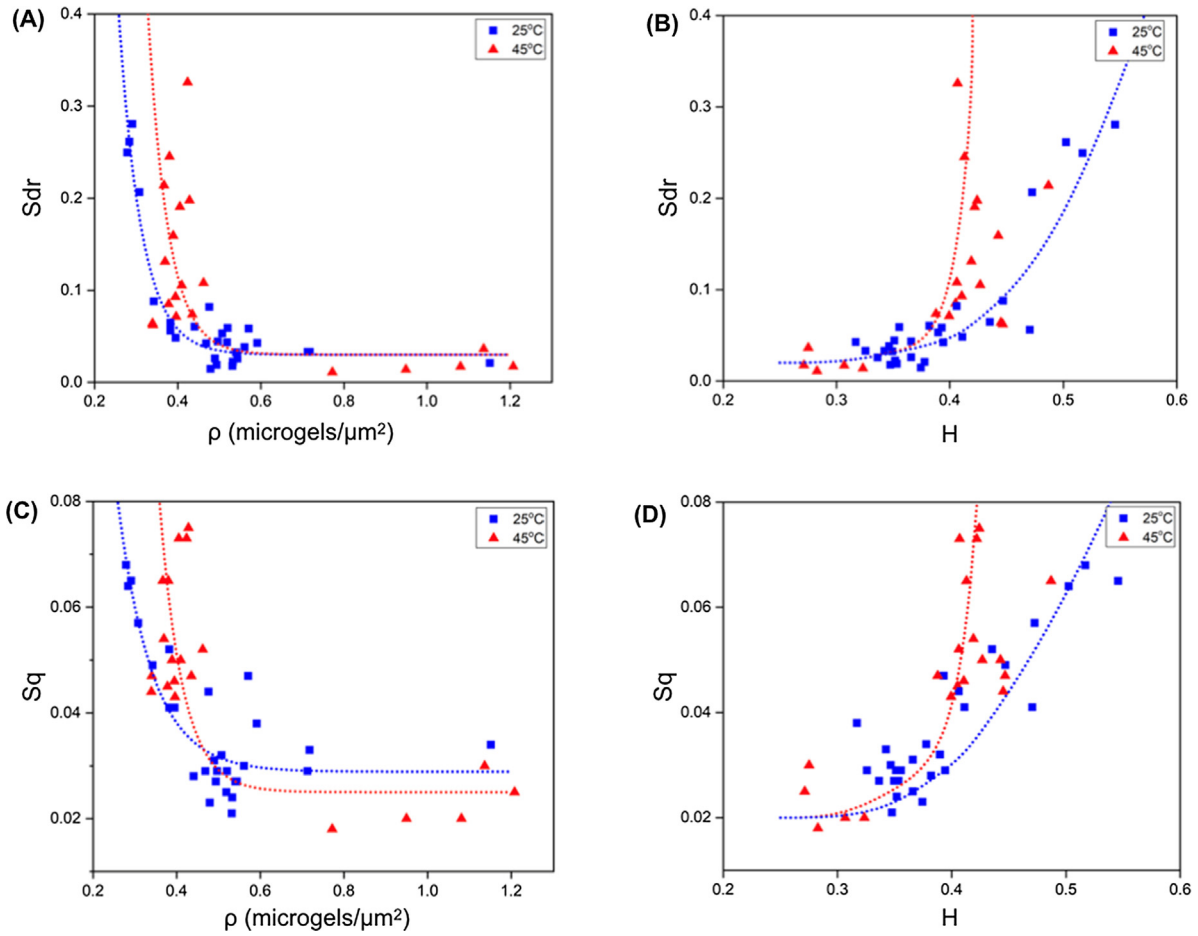

Fig. 10. Values of "developed interfacial area ratio" (Sdr, as defined by Multifile Analyzer v.2.1.2.17) *vs.* (A) microgel density (ρ) and (B) heterogeneity (H); values of "root mean square height" (Sq, as defined by Multifile Analyzer v.2.1.2.17) *vs.* (C) microgel density (ρ) and (D) heterogeneity (H). The interpolant curves (red and blue —) are added to highlight the thermal response of Sdr *vs.* ρ and Sq *vs.* ρ.

characteristics of microgel coatings, and ought to be presented as a triad to fully describe their 2D topology.

3.7. Evaluation of stimuli-responsiveness of the microgel monolayers via non-contact laser scanning microscopy

We also evaluated the thermo-responsive behavior of microgel coatings characterized by different values of ρ, H, and PE by measuring their roughness at different temperatures via non-contact surface profilometry. To this end, the various specimens were pre-conditioned at either 25 °C or 45 °C, mounted on a heat block, and imaged using a laser scanning microscope Keyence VK-X1100 (Osaka, Japan). The collected images were analyzed using the Multifile Analyzer v.2.1.2.17 (Keyence) to determine the thickness (T) of the microgel coatings by surface profilometry, as well as the dimensionless parameters "developed interfacial area ratio" (Sdr) and the "root mean square height" (Sq). Sdr expresses the additional surface area contributed by the microgels compared to the substrate area (Sdr of a flat surface is 0; when objects are present on the surface, Sdr increases), whereas Sq (standard deviation of the values of height of objects present on a surface) represents the surface roughness.

Notably, the values of T among the different coatings did not show any appreciable variation with temperature; as shown in Fig. 6S, for example, two monolayers constructed at 25 °C by spin coating 93-5-2 and 78-20-2 microgels undergo a small variation in thickness (7.8% and 11.7%, respectively) when exposed to different temperatures (25 °C *vs.* 45 °C).

The values of Sdr and Sq obtained at different temperatures are plotted against ρ (Fig. 10A and C) and H (Fig. 10B and D). Together with the expected monotonal decrease with ρ, Sdr and Sq showed an appreciable variation with temperature. Notably, both the Sdr and the Sq of coatings with low density ($\rho < 0.5$ microgel/μm^2) increase with temperature, whereas at higher density, they become independent of temperature. Conversely, Sdr and Sq showed a monotonal increase with H, with a remarkable dependence upon temperature in coatings with low homogeneity ($H > 0.4$). While portraying different surface topological characteristics of the microgel coatings, Sdr and Sq respond to thermal stimuli in a concurrent manner. As shown by Vancso and coworkers, surface-bound microgels contract from disc-like to cone-like structures upon heating [52]. Such variation can be appreciated in Fig. 6S, where the profiles of the microgel coatings at 45 °C indicate the presence of sharp entities and a higher range of ordinate values, while the profiles at 25 °C feature a smoother profile. In coatings where beads are distributed sparsely or heterogeneously, this thermally induced morphing of gel particles results in large variations in Sdr and Sq. In coatings that are densely packed or homogeneous, heating causes limited-to-no variation in these parameters. Finally, as anticipated, Sdr and Sq showed negligible correlation with PE. When averaged across a sufficiently large area, Sdr and Sq do not depend on whether microgels afford a given value of ρ or H a through geometrically regular arrangement or not. These results further confirm that ρ, H, and PE portray not only different topological characteristics of microgel coatings, but also different functional morphological properties (*i.e.*, Sdr and Sq) as well.

4. Conclusions

Polymer-based coatings that respond to environmental stimuli with reversible changes in surface morphological and physicochemical properties (*e.g.*, roughness, wettability, etc.) feature prominently in surfaces with antifouling and water-repellant behavior, biosensors, and substrates for cell culture or tissue scaffolds. Polymer nano-/micro-structures that respond to variations in temperature, pH, and conductivity of the environment are the building blocks of these systems. Key to achieving the desired functionality, however, is the understanding of the mechanisms, scale, and hierarchy of the interactions of these nano-/micro-structures among each other and with the substrate. To address this goal, this study presents a novel approach to evaluate systematically the formation, surface topology, and morphological behavior of monolayers of stimuli-responsive microgels on flat solid substrates. In the past, researchers have investigated the behavior of microgels of poly(N-isopropylacrylamide) and their derivatives on surfaces, and have established techniques to probe their behavior in response to environmental stimuli (*e.g.*, temperature, pH, and salt concentration). Our study aims to provide a new contribution in this field by addressing the effect of the physicochemical properties of the microgels and their method and environment of deposition upon the 2D morphology of the resulting monolayer. To this end, we have developed a model correlating various morphological parameters of microgel coatings with the chemical composition of the microgels as well as the deposition method (deposition *vs.* spin coating) and conditions (temperature and pH). Instrumental to this model has been the development of algorithms to derive three metrics describing distinct aspects of the surface topology of microgel arrangements, namely density (ρ), heterogeneity (H), and packing efficiency (PE). This has enabled not only the derivation of correlations guiding the construction of microgel-coated wafers with the desired property, but also a detailed investigation of how their surface morphology (3D features and roughness) changes in response to thermal stimuli. The toolbox developed and validated in this work provides valuable guidance to the design and engineering of next-generation “smart” surfaces.

CRediT authorship contribution statement

Camden Cutright: Conceptualization, Data curation, Formal analysis, Writing - original draft. **Zach Brotherton:** Conceptualization, Data curation, Formal analysis. **Landon Alexander:** Data curation. **Jacob Harris:** Data curation. **Kaihang Shi:** Data curation. **Saad Khan:** Project administration, Writing - review & editing. **Jan Genzer:** Conceptualization, Funding acquisition, Project administration, Writing - review & editing. **Stefano Menegatti:** Conceptualization, Funding acquisition, Project administration, Writing - review & editing.

Declaration of Competing Interest

The authors declare that they have no known competing financial interests or personal relationships that could have appeared to influence the work reported in this paper.

Acknowledgments

This work was partially funded by the National Science Foundation GRFP fellowship # 2017220114. The authors also wish to thank Matthew Bryant (Electrical Engineering at NC State University) for his support in preparing the image-processing codes, and Ashton Lavoie for her guidance in performing the statistical data analysis.

Appendix A. Supplementary material

Supplementary data to this article can be found online at https://doi.org/10.1016/j.apsusc.2019.145129.

References

[1] C. Neinhus, W. Barthlott, Characterization and distribution of water-repellent, self-cleaning plant surfaces, Ann. Bot. (1997) 667–677.
[2] S. Michielsen, H.J. Lee, Design of a superhydrophobic surface using woven structures, Langmuir 18 (2007) 6004–6010.
[3] B.C. Alexander, K.M. Shakesheff, Responsive polymers at the biology/materials science interface, Adv. Mater. (2006) 3321–3328.
[4] S. Ganta, H. Devalapally, A. Shahiwala, M. Amiji, A review of stimuli-responsive nanocarriers for drug and gene delivery, J. Control. Release 126 (3) (Mar. 2008) 187–204.
[5] S. Miao, W. Zhu, N. Castro, L. Jinsong, L. Zhang, Four-dimensional printing hierarchy scaffolds with highly biocompatible smart polymers for tissue engineering applications, Tissue Eng. 22 (10) (2016) 952–964.
[6] L. Riley, L. Schirmer, T. Segura, ScienceDirect Granular hydrogels: emergent properties of jammed hydrogel microparticles and their applications in tissue repair and regeneration, Curr. Opin. Biotechnol. 60 (2019) 1–8.
[7] M. Karg, et al., Nanogels and microgels: from model colloids to applications, recent developments, and future trends, Langmuir 35 (2019) 6231–6255.
[8] E. Kharlampieva, I. Erel-unal, S.A. Sukhishvili, Amphoteric surface hydrogels derived from hydrogen-bonded multilayers: reversible loading of dyes and macromolecules, Langmuir 4 (2007) 175–181.
[9] J.A. Jaber, J.B. Schlenoff, Polyelectrolyte multilayers with reversible thermal responsivity, Macromolecules (2005) 1300–1306.
[10] L.E. Bromberg, E.S. Ron, Temperature-responsive gels and thermogelling polymer matrices for protein and peptide delivery, Adv. Drug Deliv. Rev. 31 (1998) 197–221.
[11] J. Lutz, K. Weichenhan, O. Akdemir, A. Hoth, About the phase transitions in aqueous solutions of thermoresponsive copolymers and hydrogels based on 2-(2-methoxyethoxy) ethyl methacrylate and oligo (ethylene glycol) methacrylate, Macromolecules (2007) 2503–2508.
[12] S. Nayak, S.B. Debord, L.A. Lyon, Investigations into the deswelling dynamics and thermodynamics of thermoresponsive microgel composite films, Langmuir 12 (2003) 7374–7379.
[13] R. Lupitskyy, Y. Roiter, C. Tsitsilianis, S. Minko, From smart polymer molecules to responsive nanostructured surfaces, Langmuir 12 (2005) 8591–8593.
[14] A. Sidorenko, T. Krupenkin, A. Taylor, P. Fratzl, Reversible switching of hydrogel-activated nanostructures into complex micropatterns, Science (80-.) 315 (5811) (2019) 487–490.
[15] A. Sidorenko, J. Aizenberg, Controlled switching of the wetting behavior of biomimetic surfaces with hydrogel-supported nanostructures, J. Mater. Chem. (2008) 3841–3846.
[16] N. Houbenov, S. Minko, M. Stamm, Mixed polyelectrolyte brush from oppositely charged polymers for switching of surface charge and composition in aqueous environment, Macromol. Rapid. Commun. (2003) 5897–5901.
[17] C.D. Sorrell, M.C.D. Carter, M.J. Serpe, Color tunable poly (N-isopropylacrylamide)-co-acrylic acid microgel – Au hybrid assemblies, Adv. Funct. Mater. (2011) 425–433.
[18] E.C. Cho, J. Lee, K. Cho, Role of bound water and hydrophobic interaction in phase transition of poly(N-isopropylacrylamide) aqueous solution, Macromolecules (2003) 9929–9934.
[19] C. Wu, A comparison between the ‘ coil-to-globule ’ transition of linear chains and the ‘“ volume phase transition ”’ of spherical microgels, Polymer (Guildf) 39 (19) (1998) 4609–4619.
[20] D. Schmaljohann, Thermo- and pH-responsive polymers in drug delivery, Adv. Drug Deliv. Rev. 58 (15) (Dec. 2006) 1655–1670.
[21] V.A. Online, et al., pH and thermo responsive poly(N-isopropylacrylamideco-acrylic acid derivative) copolymers and hydrogels with LCST dependent on pH and alkyl side groups, J. Mater. Chem. B (2013) 5578–5587.
[22] Q. Zhang, C. Weber, U.S. Schubert, R. Hoogenboom, Thermoresponsive polymers with lower critical solution temperature: from fundamental aspects and measuring techniques to recommended turbidimetry conditions, Mater. Horiz. (2017).
[23] X. Yin, A.S. Hoffman, P.S. Stayton, Poly(N-isopropylacrylamide-co-propylacrylic acid) copolymers that respond sharply to temperature and pH, Biomacromolecules 7 (5) (2006) 4–8.
[24] M.J. Snowden, B.Z. Chowdhry, B. Vincentb, G.E. Morrisb, Colloidal copolymer microgels of N-isopropylacrylamide and acrylic acid: pH, ionic strength and temperature effects, J. Chem. Soc 92 (24) (1996) 5013–5016.
[25] K. Kratz, T. Hellweg, W. Eimer, Influence of charge density on the swelling of colloidal poly (N-isopropylacrylamide-co-acrylic acid) microgels, Colloids Surf. A, c (2000) 137–149.
[26] J.J. Chen, A.L. Ahmad, B.S. Ooi, Thermo-responsive properties of poly (N-isopropylacrylamide-co-acrylic acid) hydrogel and its effect on copper ion removal and fouling of polymer-enhanced ultrafiltration, J. Memb. Sci. 469 (2014) 73–79.
[27] Y. Lu, S. Proch, M. Schrinner, M. Drechsler, M. Ballauff, Thermosensitive core-shell microgel as a ‘“ nanoreactor ”’ for catalytic active metal nanoparticles, J. Mater. Chem. (2009) 3955–3961.
[28] P. Bawa, V. Pillay, Y.E. Choonara, L.C. du Toit, Stimuli-responsive polymers and their applications in drug delivery, Biomed. Mater. 4 (2) (Apr. 2009) 022001.
[29] E. Sproul, S. Nandi, S. Chee, A. Brown, Development of biomimetic antimicrobial platelet-like particles comprised of microgel nanogold composites, Regen. Eng. Transl. Med. (2019).
[30] M.A. Lifson, J.A. Carter, B.L. Miller, Functionalized polymer microgel particles enable customizable production of label-free sensor arrays, Anal. Chem. (2015).
[31] K.C. Clarke, A.M. Douglas, A.C. Brown, T.H. Barker, L.A. Lyon, Current opinion in

colloid & interface science colloid-matrix assemblies in regenerative medicine, Curr. Opin. Colloid Interface Sci. 18 (5) (2013) 393–405.
[32] F. Review, P. Kodlekere, A. Pich, Functional microgels for the decoration of biointerfaces, ChemNanoMat (2018) 889–896.
[33] S. Schmidt, H. Motschmann, T. Hellweg, R. von Klitzing, Thermoresponsive surfaces by spin-coating of PNIPAM-co-PAA microgels: a combined AFM and ellipsometry study, Polymer (Guildf) 49 (3) (2008) 749–756.
[34] S. Schmidt, T. Hellweg, R. Von Klitzing, Packing density control in P(NIPAM-co-AAc) microgel monolayers: effect of surface charge, pH, and preparation technique, Langmuir 109 (7) (2008) 12595–12602.
[35] M. Seeber, B. Zdyrko, R. Burtovvy, T. Andrukh, C. Tsai, J.R. Owens, Surface grafting of thermoresponsive microgel nanoparticles, Soft Matter (2011) 9962–9971.
[36] A.C. Brown, et al., Ultrasoft microgels displaying emergent platelet-like behaviours, Nat. Mater. 13 (12) (2014) 1108–1114.
[37] Y. Ko, J. Genzer, Spontaneous degrafting of weak and strong polycationic brushes in aqueous buffer solutions, Macromolecules 52 (2019) 6192–6200.
[38] T. Wu, M. Tomlinson, K. Efimenko, J. Genzer, A combinatorial approach to surface anchored polymers, J. Mater. Sci. 8 (2003) 4471–4477.
[39] A. Joshi, S. Nandi, D. Chester, A. Brown, M. Muller, Study of poly(N-isopropylacrylamide-co-acrylic acid) (pNIPAM) microgel particle induced deformations of tissue-mimicking phantom by ultrasound stimulation, Langmuir 34 (4) (2018) 1457–1465.
[40] K. Shi, K. Gu, Y. Shen, D. Srivastava, E.E. Santiso, K.E. Gubbins, High-density equation of state for a two-dimensional Lennard-Jones solid, J. Chem. Phys. 148 (2018).
[41] G.C. Chi, G.S. Cargill, Structural characterization of amorphous electrodeposited cobalt-phosphorus alloys, J. App. Phys. 50 (4) (1979) 2713–2720.
[42] L. Charlet, A. Manceau, Structure, formation and reactivity of hydrous oxide particles; insights from X-ray absorption spectroscopy, Environmental Particles II, Harvard, 2018.
[43] V.V.T. Doan-Nguyen, S.A.J. Kimber, D. Pontoni, D. Reifsnyder-Hickey, B.T. Diroll, X. Yang, M. Miglierini, C.B. Murray, S.J.L. Billinge, Bulk metallic glass-like scattering signal in small metallic nanoparticles, ACS Nano 8 (6) (2014) 6163–6170.
[44] J. Ward, E. Ollmann, E. Maxey, L.A. Finney, X-ray absorption spectroscopy of metalloproteins, Meth. Mol. Biol. 1122 (2014) 171–187.
[45] P. Wochner, C. Gutt, T. Autenrieth, T. Demmer, V. Bugaev, A. Díaz Ortiz, A. Duri, F. Zontone, G. Grübel, H. Dosch, X-ray cross correlation analysis uncovers hidden local symmetries in disordered matter, PNAS 106 (28) (2009) 11511–11514.
[46] E.B. Sirota, H.D. Ou-Yang, S.K. Sinha, P.M. Chaikin, J.D. Axe, Y. Fujii, Complete phase diagram of a charged colloidal system: a synchrotron x-ray scattering study, Phys. Rev. Lett. 62 (13) (1989) 1524.
[47] J.C. Crocker, D.G. Grier, Methods of digital video microscopy for colloidal studies, J. Coll. Int. Sci. 179 (1) (1996) 298–310.
[48] E. Gavagnin, J.P. Owen, C.A. Yates, Pair correlation functions for identifying spatial correlation in discrete domains, Phys. Rev. E 97 (6) (2018).
[49] C.J. Dibble, M. Kogan, M.J. Solomon, Structure and dynamics of colloidal depletion gels: coincidence of transitions and heterogeneity, *Phys. Rev. E* 74 (4) (2006).
[50] C. Gao, S.D. Kulkarni, J.F. Morris, J.F. Gilchrist, Direct investigation of anisotropic suspension structure in pressure-driven flow, *Phys. Rev. E* 81 (4) (2010).
[51] P. Varadan, M.J. Solomon, Direct visualization of long-range heterogeneous structure in dense colloidal gels, Langmuir 19 (3) (2003) 509–512.
[52] O. Tagit, N. Tomczak, G.J. Vancso, Probing the morphology and nanoscale mechanics of single poly (N-isopropylacrylamide) microgels across the lower- critical-solution temperature by atomic force microscopy, Small 117607 (1) (2008) 119–126.